3D-printed electroactive polymer force-actuator for large and high precise optical mirror applications

Kritsadi Thetpraphi, Waroot Kanlayakan, Suphita Chaipo, Gil Moretto, Jeff Kuhn, David Audigier, Minh Quyen Le, Pierre-Jean Cottinet, Lionel Petit, Jean-Fabien Capsal

3D-Printed Electroactive Polymer Force-Actuator for Large and High Precise Optical Mirror Applications

Kritsadi Thetpraphi[1], Waroot Kanlayakan[1#], Suphita Chaipo[1#], Gil Moretto[2], Jeff Kuhn[3], David Audigier[1], Minh Quyen Le[1], Pierre-Jean Cottinet[1], Lionel Petit[1], and Jean-Fabien Capsal[1*]

[1] *Univ Lyon, INSA-Lyon, LGEF, EA682, F-69621, Villeurbanne, France*
[2] *Centre de Recherche Astrophysique de Lyon (CRAL), 9 avenue Charles André, 69230 Saint-Genis-Laval, France*
[3] *University of Hawaii's Institute for Astronomy, 34 Ohia Ku St, Pukalani, Maui, HI, USA*
Master Degree Internships between INSA/Lyon and Prince of Songkla University, Songkhla, Thailand.

* Corresponding author: jean-fabien.capsal@insa-lyon.fr; Tel.: +33-4 72 43 88 33

Abstract:

We describe a new development for a full 3D-printed-force actuator based on an advanced electroactive polymer (EAP) dedicated to large and live optical mirror applications, i.e., Live-Mirror Project (https://www.planets.life/live-mirror). The thin-film casting method was used to additively manufacture actuators, and we developed an integrating 3D printing technology to the EAP force-actuator production. Our 3D-printed actuator consists of the plasticized terpolymer layer (polyvinylidene fluoride-trifluoroethylene-chlorotrifluoroethylene (PVDF-TrFE-CTFE) doped with diisononyl phthalate (DINP) plasticizer) sandwiched between two electrodes layers made of conductive terpolymer carbon black (CB) composite. The conductive CB layers were developed here to have a high electrical conductivity that can be used under significant voltage. We also made compatible blends with an actuator layer based on DINP polymer. Several fully 3D-printed EAP proof-of-concept actuator configurations were printed on a two-millimeters thick flat glass, i.e., an optical mirror surface. Its electromechanical performance was analyzed as a function of actuator volume, layer number, and electrical field intensity.

Keywords: Electroactive doped polymer, 3D printing, EAP force-actuator, active optical mirror, active control of glass deformation, flexible printed materials, optimization of printed electrodes.

I. Introduction

3D printing technology offers several advantages for diverse materials processing such as rapid prototyping making use of an object from a computer-aided design (CAD). Additive manufacturing developments have improved and advanced 3D-printer technology by providing commercially customized products to overcome the time-consuming process of complex shape products [1,2]. In particular, *flexible printed materials* have been attractive for large-area electronic devices, e.g., wearable electronics of 3D tactile sensors [3,4], printed CNC (Computerized Numerical Control) process scaffolds for specific cell integration [5], polymer photo-detectors [6], and 3D-printed soft dielectric elastomer actuators [7,8].

Material extrusion printing is a common technique used to build a structure of any desired shape of dielectric elastomer [9]. This 3D printing process allows various kinds of material to be extruded to build up a platform along a predetermined path. The difficulty of this printing technique is the use of a fluid or solution-based material that requires the control of a variety of parameters that characterize the material/solvent: evaporation rate, viscosity grade, flow regulation, mold temperature, chemical compatibility for multi-material structure. These must be tuned to achieve an efficient and reproducible printing process. We recently reported the possibility of using a casting method to produce an EAP-based modified terpolymer as a force-actuator system for a highly accurate optical surface deformation and correction [10,11].

To fabricate active optics in Live-Mirror applications, we used the EAP that can shape and/or deform the mirror surface thanks to its electromechanical conversion. Recently, Thetpraphi *et al.* [11] reported a handcrafted prototype [11], i.e., a film-casting actuator production. The design is a shear actuator (thin-film EAP glued with a single glass plate). To develop a unique force-actuator device that can be precisely integrated into certain mirror positions, we opted for an extrusion-based 3D printing technique through Hyrel System 30M 3D printer [12]. Based on this approach, it is possible to overcome the interface-related problems, which principally caused by a deficiency in force transferring between EAP to a glass surface (handcrafted prototype). Considering the customized electrode and actuator patterns, it is necessary to design each actuator matching individual optical surfaces. Thus, the integration of additive manufacturing is very important to fabricate a large area, unique and precise actuator to fulfill the requirement of the future Live-Mirror application. Additionally, the provision of extrusion-based 3D printing techniques will be essential for developing a wide range of smart mirror fabrication. In other words, a specified actuator shape is needed to accurately integrate it into certain mirror positions, from small-scale (lab-scale) to wide-reaching innovative applications. In this paper, we aim to fabricate a force-actuator using 3D printing technology and optimize its electromechanical performance with several configurations. The main purpose involves demonstrating the proof-of-concept of 3D printing multilayer EAP included with customized electrodes. Although researchers are actively investigating 3D printing technology, the full-printed actuator is still rather limited today because of incompatibility between polymer and electrode layers [1,7,13].

3D printing of the conductive electrode layer is the most challenging. Most conductive metallic inks require a sintering process to reach a good conductive range and bulk content. The sintering procedure of some conductive inks, e.g., silver ink, is 150°C and above. Nonetheless, stretchable electronic applications need to be fabricated at moderate temperatures to prevent sample damage and/or degradation of the incorporated materials. Dearden *et al.* [14] demonstrated the possibility of reducing the sintering temperature of organometallic inks lower than 150°C. Another option to avoid operating materials under high temperatures is to use intrinsically conductive polymer (ICP) and/or conductive polymer composite (CPC). Even though ICP and CPC exhibit lower conductivity than metallic ink, their advantages in terms of compliance, cost, resilience, density, and biocompatibility have attracted a great deal of research interest.

Recent studies have focused on the improvement of electrical conductivities of ICP and CPC for flexible actuator and sensor applications. Kayser *et al.* [15] described a stretchable scaffold made from an intrinsically synthesizing variant of PEDOT: PSS to develop soft and skin-like semiconductors and conductors. Cochrane *et al.* [16] used the evoprene 007 (EVO) ($T_m \approx 82$°C) for polymer hosts filled with carbon black (CB) powder as a smart flexible sensor. Kumar *et al.* [17] reported on an elastomer ethylene-vinyl acetate EVA ($T_m \approx 75$°C) doped with graphite and CNC-assisted manipulated as a three-dimensional flexible electrically conductive structure for soft robotics applications. Hence, ICP and CPC could intimate the printability to mitigate solvent evaporation under low temperature showing their high potential in applications of soft electronic devices. Numerous parameters must be considered to demonstrate the printability of materials in additive manufacturing, e.g., compatibility between conductive inks and substrate or cooperative materials, wettability (substrate-polymer), surface bonding (polymer-polymer), curing temperature, etc. Considering all such challenging complexities, we developed here a conductive ink made from P(VDF-TrFE-CTFE) fluorinated terpolymer doped with CB nanoparticles (Vulcan® XC72R) that is adaptable for extrusion 3D printing.

II. Fabrication process and method of characterization

i. Material design and 3D printing setup

The EAP solution is prepared in a liquid form ready for printing by dissolving terpolymer granules in methyl ethyl ketone (MEK, also known as butanone) solvent at a fraction of 20.25% wt. The fully printed force-actuator proof of concept includes the 3D printing of all layers, i.e., consisting of the EAP plasticized terpolymer sandwiched between the two terpolymer/CB composite (top and bottom) layers. Figure 1 shows the extrusion-based 3D printing setup: (A) the electrode circular-shaped layers are printed with different diameters, and the EAP layer is designed to have a larger area than the electrode ones to avoid electrical arcing between these electrodes under high voltage; (B) the material extrusion setup consisted of a modular head sterile cold flow (SDS) [12] extruders (at room temperature); and (C) a glass platform that allowed translation in x-, y-, and z-directions. Here, we used commercial float glasses with 110mm-diameter and 2mm-thickness as the optical substrate. The mechanical properties of the glass are found on [18]. In the preparation process, the actuator was printed on one side of the glass (called "back surface") while the other side was referred to as the control optical surface (called "front surface"). The front surface of the glass coated with a gold layer of 25nm thick allows obtaining its deformation measurement. On the other hand, this architecture prevents the reflection from the back surface of the glass. Consequently, the optical properties of EAP would not much affect the glass deformation, which is therefore not taken into consideration for the mirror application.

The extruder used in this work allows the use of sterile syringes at room temperature. The prepared solution was put in a syringe and printed at room temperature with a speed of 800 mm/min through a nozzle of 14G for the EAP, and 18G for the electrode. Using a smaller nozzle for printing electrodes leads to higher pattern precision, particularly in the case of complex shapes. Whatever actuator dimension, the printing configuration was carried out with 100% filling density in order to achieve the best material performance. To completely evaporate the solvent from the full-printed actuator (consisting of three layers of electrode/EAP/electrode), samples were put into an oven with temperature-controlled of 102°C for 2h, then cooled down slowly for 16h to room temperature. The average thickness of the whole sample is approximately 130 µm including 90-100 µm for the EAP layer and 15-20 µm for the electrode circular-shaped layer. A control-software 3D printing code (Repetrel by Hyrel [12]) is used to control parameters such as tuning, speed, and pressure. This allows one to print the EAP force-actuator in optimized configurations similar to those in a COMSOL simulation.

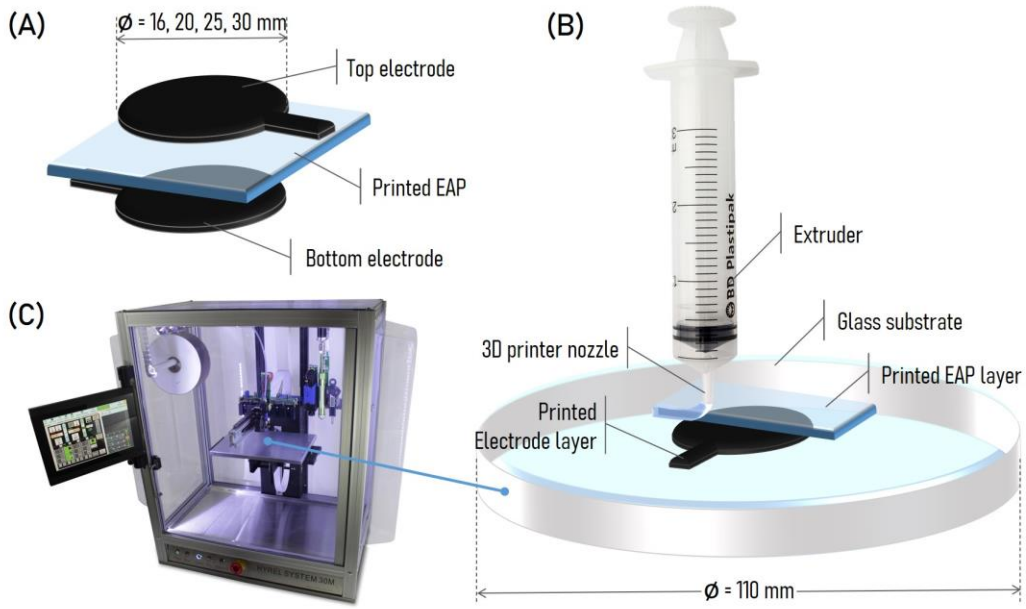

Figure 1. *The full-printed actuator based EAP:* ***(A)*** *force-actuator made of plasticized terpolymer switched between two electrodes layers of terpolymer/CB composite;* ***(B)*** *3D printing setup of actuator layers using* ***(C)*** *the commercial System 30M Hyrel 3D printer* [12].

Thetpraphi *et al.* [10,11,19] demonstrated the high potential of the stacked multilayer actuator configuration, which successfully enhances the dielectric properties as well as the electromechanical coupling of the EAP materials. Here, a stacked actuator consisting of three printed layers (i.e., one active layer based EAP and two electrode layers-based conductive-ink) was investigated corresponding to layer-by-layer extrusion (Figure 1B). Printed electrodes with a conductive polymer ink revealed their high potential to implement flexible and stretchable electronic devices such as nanoparticles colloid suspension, organometallic inks, carbon nanotube, graphene oxide, and reactive inks [20].

The first full-printed EAP prototype was fabricated on a single glass blank working in a shear-mode actuator under various configurations. Such a single-layer actuator consists of a single EAP layer (terpolymer doped 8 wt%DINP), and two electrode layers (terpolymer doped 5wt% CB composite). Figure 2 shows two different shear prototype configurations: (1) the full-printed multi-actuator prototype has four individual single-layer actuators as shown in Figure 2A; (2) the full-printed single actuator prototype has one actuator located at the central glass substrate (Figure 2B).

Since the 3D printing process is somehow analog to the thin-film casting method, we presumed that the surface roughness of samples made by the new 3D technique is relatively smooth and thus would not much affect the actuator performance. Indeed, both methods lead to a fabrication of thin film in which the EAP and/or the electrode were fully coated on the glass substrate without any intermediary adhesive layer. The SEM images (FlexSEM 1000II) illustrating the surface roughness of those samples fabricated by 3D printing or casting process are presented in Figure 3. The morphological observations of the film surface in both techniques are homogeneous and undifferentiated. As observed in Figure 3 (A2) and (B2), few tiny straight lines of ~2µm-width appear over both film surfaces, which is possibly originated from some inevitable defects during the elaboration process.

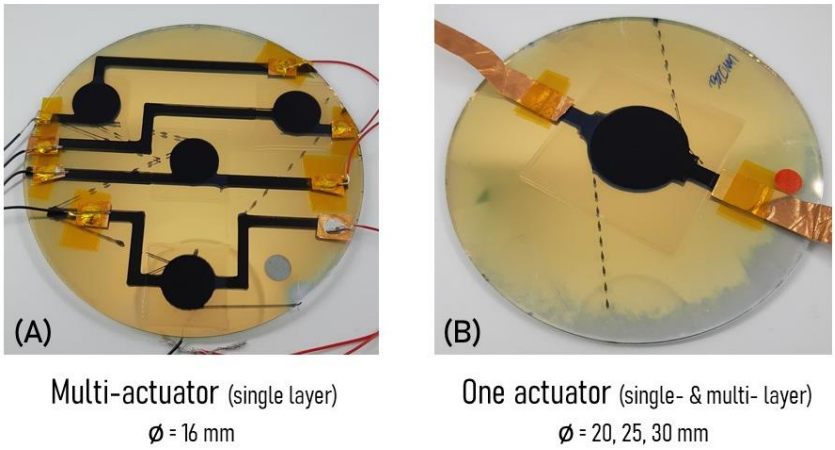

142

143 ***Figure 2****. The full-printed actuator prototype:* ***(A)*** *Multi-actuator configuration consisting of four actuators with a 16-mm-diameter*
144 *electrode; and* ***(B)*** *single actuator at the central mirror glass which has three different electrodes sizes. The single actuator is printed as a*
145 *multilayer stacked actuator by successively depositing 3 layers of electrode/EAP/electrode.*

146

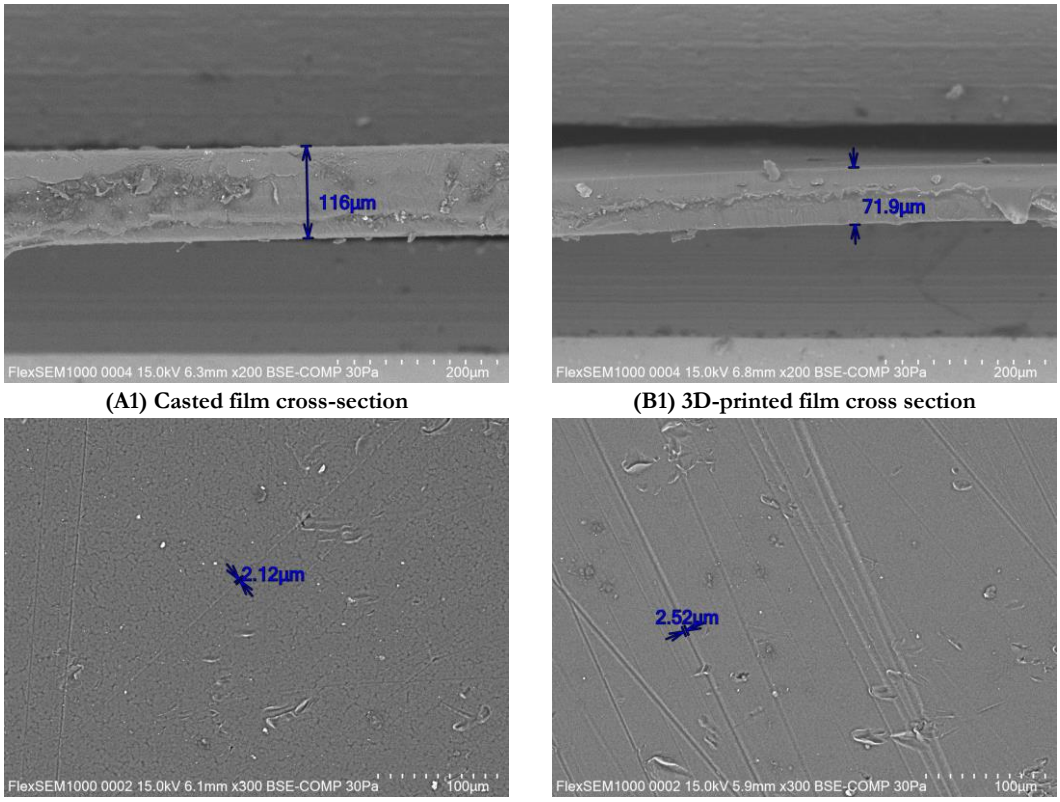

(A1) Casted film cross-section **(B1) 3D-printed film cross section**

(A2) Casted film surface **(B2) 3D-printed film surface**

147 ***Figure 3****. SEM micrographs of plasticized terpolymer thin films prepared by (A1-2) film casting method, and (B1-2) 3D-printed*
148 *method.*

149 ### ii. Electrical characterization of CB electrode layers

150 Here a conductive polymer composite (CPC) was selected to print the two electrode layers of the
151 actuator design (Figure 1A). This approach uses the same polymer host between the electrode and EAP
152 actuator layer. It reduces the complexity of ink preparation and avoids material compatibility issues. Because
153 the deformation needed to shape the mirror is less than 1%, we exclusively focus on the linear elastic
154 domain [21] of the terpolymer in this investigation. Based on the linear stress/strain curve characterized in

our previous work [22], it is possible to deduce the Young modulus of the plasticized terpolymer, i.e. approximately 30 MPa. This property is perfectly suitable for dedicated optical applications. Indeed, the EAP is flexible enough to deform itself, but it is somehow strong enough to generate sufficient force to shape the mirror. A compromise between force and deformation makes terpolymer one of the most appropriate choices for the design of actuator devices [21]. It is worth noting that the low percentage of CB powder dispersed into the terpolymer matrix would not significantly modify its Young modulus. For more details about the mechanical properties of terpolymer composites doped with different DINP or CB fraction content, the readers can refer to [11,23–25].

The CB particles were well-dispersed in the Terpolymer/MEK solution thanks to an ultrasonic probe (UP400S from Hielsher). Figure 4 outlines the S-shaped electrical conductivity of the printed Terpolymer/CB ink with different weight fractions of CB particles. Beyond 1 wt% of CB content, the conductivity drastically increases confirming that the percolation threshold of the composite is approximately 4 -5 wt%. At 5 wt% of CB filler, the electrode layer became conductive and reached a small overshoot of 0.57 ± 0.14 S/m. Beyond the percolation transition, the conductivity of the composite ink somehow dropped and was in the saturation regime. Such a slight decrease in the electrical conductivity can be explained by the fact that higher CB concentration probably generated a cluster of particle agglomeration, leading to reduced efficacy in the conductive pathway. All these experimental results indicate that the transition from insulation polymer to high conductivity composite depends on the formation of an interconnected conductivity network. In other words, superior conductivity arises from the high dispersion and the formation of a network structure in the polymer matrix. It can be concluded that many factors comprising intrinsic electrical properties of the doped particles, aspect ratio, dispersion state, and contact resistance between particle/particle and particle/matrix might greatly affect the electrical conductivity of the whole composites [26,27].

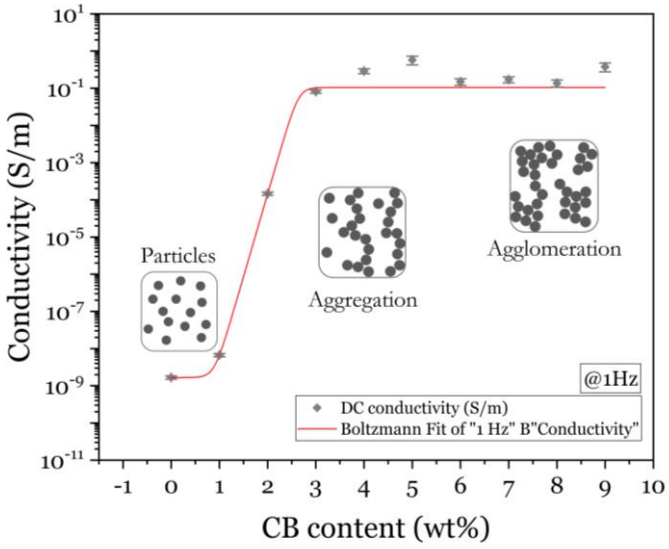

Figure 4*. The electrical conductivity of terpolymer filled with carbon black (CB) particles accurately obtained from the dielectric broadband spectroscopy (DBS) system operated at a sinusoidal voltage of 1V amplitude and 1 Hz frequency.*

Considering the dispersion of CB particles in the polymer matrix, Figure 5 presents micrograph images via scanning electron microscope (SEM, FlexSEM 1000II) analysis of samples elaborated with 5% and 9% of CB concentration. A higher agglomeration of CB particles is observed on the 9% composite, which is consistent with the fact that its electrical conductivity is lower than the one of the 5%. To some extent, the conductivity slightly increases again at 9%, i.e., maybe due to measurement uncertainties and random particle formation in the conductivity network.

Controlling cluster formation of CB composite above percolation is complex, especially when particles are dispersed randomly. In this study, we demonstrated that the electrical conductivity of the printed electrodes is sufficient for a satisfying actuation response. Due to the low operating frequency, the EAP has such a high electrical impedance as compared to the electrodes. Finally, the 5wt% of CB composite is the most favorable material to be used as the printable electrode, because of its homogeneous dispersion in the polymer host, as well as its good electrical conductivity at the low percentage of doping filler. Furthermore, the 5wt% EAP layer somehow remains a relatively low Young modulus with respect to the 9% counterpart [23,25,28].

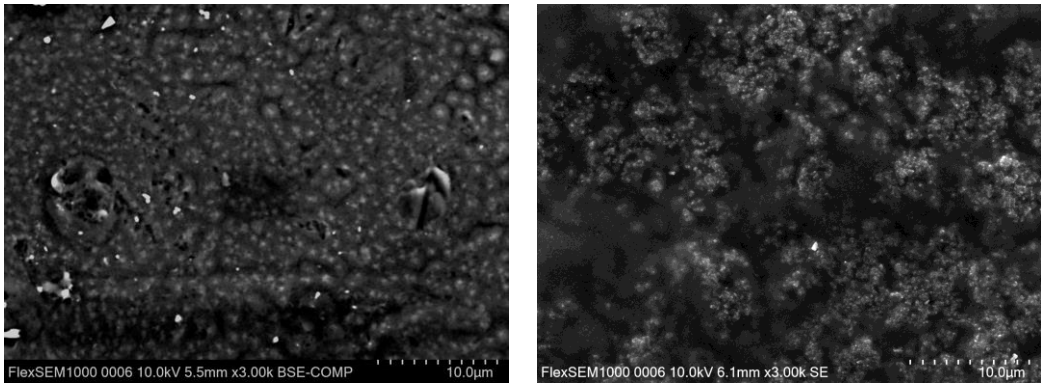

(A) 5% CB **(B) 9% CB**

Figure 5. *SEM micrographs of the terpolymer doped with CB (A) 5wt% and (B) 9wt% respectively. Compared to the 5% CB concentration, the 9% counterpart seems to provide a larger cluster of CB particle agglomeration, creating the disconnected path within the polymer matrix.*

Figure 6A shows the electrical conductivity evolution of CB composite above the percolation regime in a large frequency range of [1 Hz, 1 MHz]. Whatever the weight fraction of CB powders, the conductivity values are stable under low frequencies while being dropped over high frequencies of around 10^5 Hz. Despite this non-perfect conductive behavior, the terpolymer/CB composite remains an interesting solution for 3D printing electrodes because of its good conductivity and high adaptability to the EAP actuator layer.

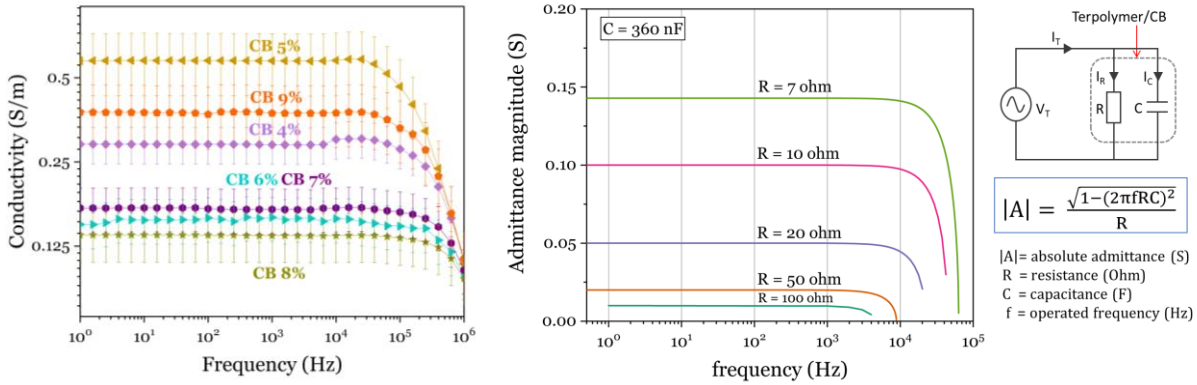

(**A**) (**B**)

Figure 6. *The electrical conductivity of terpolymer doped with CB composite above the percolation region characterized as a function of frequency:* ***(A)*** *the experimental characterization measured with Solartron; and* ***(B)*** *the admittance $|A|$ evaluation calculated through the real capacitance and the resistance values of terpolymer/CB composite-based RC parallel circuit.*

The polymer composite is a capacitive-like material that could be modeled as an RC parallel circuit [29,30]. Its admittance value **A** (Siemen: S) is determined according to Figure 6B. Similar to the conductivity property, the admittance magnitude is also frequency-dependent where a significant fall has been observed

under high frequencies. The identification between the experimental data and the analytical model of the EAP's admittance allows us to predict the RC components of the terpolymer doped with high CB concentration (4%-9% by mass). The estimated resistance and capacitance of the 64 μm-thick films are approximately 2-10 ohms and 360 nF, respectively.

The conductivity evolution is given by the experimental measurement (Figure 6A) and the theoretical modeling (Figure 6B). It behaves as a low-pass filter response where the cut-off frequency is around 73 ± 5 kHz. The small discrepancy between experiment and model is possibly due to the composite particle agglomeration, which provides an inconsistent resistance value to the material composite. Here, we operate the polymer actuator in a low-frequency range (lower than 50 mHz), which is compliant to large and accurate optical active surface mirror low-frequency correction and not a high bandwidth requirement. This means that the effect of the AC filter at a very high-frequency range could be neglected (at least for this application).

The main goal here is to achieve active shape control with many-degree-of-freedom force actuators created by an additive 3D printing-based technology. Based on an optimized EAP force actuator system in a sandwich of specified shaped/slumped glass surfaces, it is possible to create a novel actively controlled ***hybrid meta-material*** with a superior stiffness-to-density ratio dedicated to optical quality mirror surfaces.

iii. Dielectric characterization of force Actuators

The dielectric permittivity is one of the most important intrinsic parameters of an EAP. A higher dielectric constant implies a higher efficiency of the mechanical energy density for actuation performance [21]. The full-printed actuator ability was assessed by their dielectric characterization as a function of frequency. Figure 7 illustrates the relative permittivity real part (ε_r) as well as the loss factor (**Tanδ**) of the modified terpolymer under a large frequency range of 0.1 Hz – 1 MHz. When the DINP plasticizer is incorporated within the terpolymer matrix, it strongly promotes the mobility of dipolar relaxation and thus enhances the dielectric permittivity [22,24,31]. However, too much DINP quantity could decrease the electrical strength of the blend producing dielectric breakdown. Thetpraphi *et al.* [11] reported that the terpolymer must be integrated with an 8-10 wt% plasticizer to get the best trade-off between the dielectric property and the breakdown strength. Here, terpolymer doped with 8 wt % DINP was employed. Figure 7 shows that the full-printed multilayer actuator leads to substantial enhancement in dielectric permittivity concerning the neat terpolymer (ε_r ~70), i.e., 150 for the single-layer actuator and 450 for the three-layer actuator, respectively.

Another key parameter relating to actuator performance is dielectric loss. As indicated in Figure 7, the resulting loss tangent of the fabricated composite is relatively high, which might originate from the low conductivity (higher resistivity) of the printed electrode layers. Our printed electrodes are not perfectly conductive versus an ideal electrode (e.g., one made of gold or copper). This is because their conductivity (i.e. 0.5 S/m shown in Figure 4) is the same order of magnitude as that of typical semiconductors like Si and Ge. The actuator with high losses can be minimized by improving the conductivity of the printed electrode. Live-Mirror systems are operated at very low frequency (~50 mHz), and the loss issue at high frequency can be neglected. In contrast, the loss is principally generated by the Ohmic conduction mechanism under a quasi-static regime as in our application [32]. Pedroli *et al.* proposed a different approach to reducing the conduction loss effect in the EAP. This matter will be considered in future studies to improve the conductive property of our printed electrode.

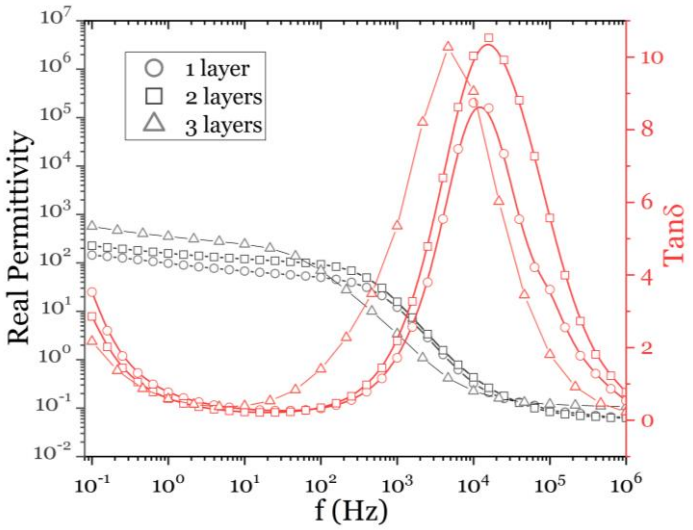

Figure 7. *The dielectric broadband spectroscopy of full-printed EAP with different layers operated under a sinusoidal voltage of 1 V_{AC}-amplitude at room temperature. The gray curves are related to the real permittivity while the red curves are dedicated to the* $\tan\delta$ *losses.*

III. Customized Full Printed Force-Actuator — Live Mirror Application

The full-printed actuator was prepared through a shear prototype configuration that uses the advantage of the transversal strain (S_{31}) generated by the EAP actuator. This mechanical transverse expansion creates a shear force that can shape the glass surface. After electrical polishing, the system relied on the actuator configuration. An effective electrical polishing implies high DC fields swept from 10-30 V/µm applied directly through the electrode layers printed on the backside of the glass substrate. The control surface Sc is where the EAP force-actuators are also 3D printed in a stacked configuration (Figure 2). The Sc deformations (overall surface wavefront fringes) are measured through a laser interferometer instrument (Figure 8). These measurements are front-side reflective mirrors. The fact is that the front surface is covered by metallic deposition, while the EAP actuator is translucent and its optical properties [33,34] do not affect the mirror deformation. On one hand, the measurement was performed on the front-side mirror. This means that the incident and reflected rays driven by the Zygo interferometer appear only on the front-side of the mirror called the control surface (Sc), correspondingly. As observed in Figure 8, actuators were fixed on the backside of the mirror where the interaction with light rays is not significant. In other words, the EAP layer does not have an impact or absorb this quality of the reflective coating on the front side. Consequently, the EAP actuator was entirely operated the glass deformation without being influenced by light.

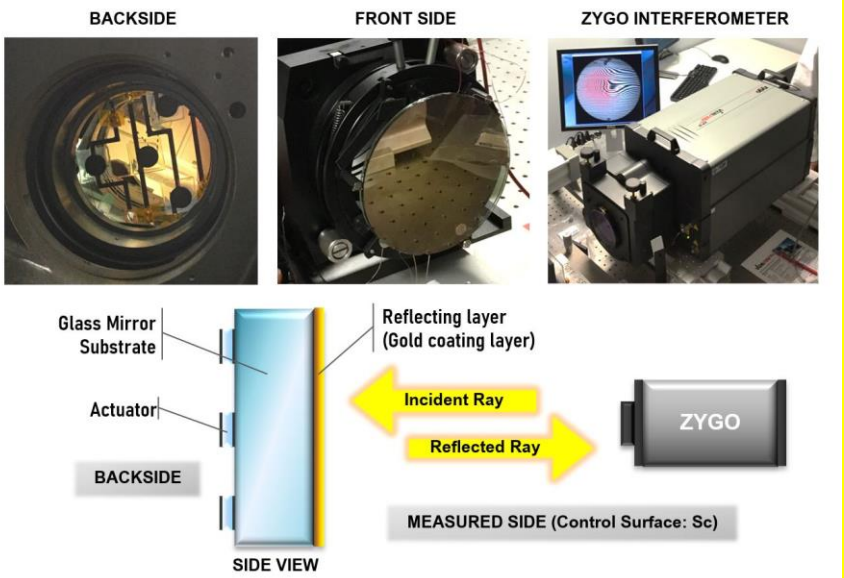

Figure 8. *The experimental setup of the glass surface deformation presents the measurement configuration: backside, front side, and side view of the mirror prototype. The control surface: Sc (front surface) coated with gold layer was faced to the laser interferometer (Zygo Verifire™) to obtain its deformation when actuators, fixed on the backside, were actuated.*

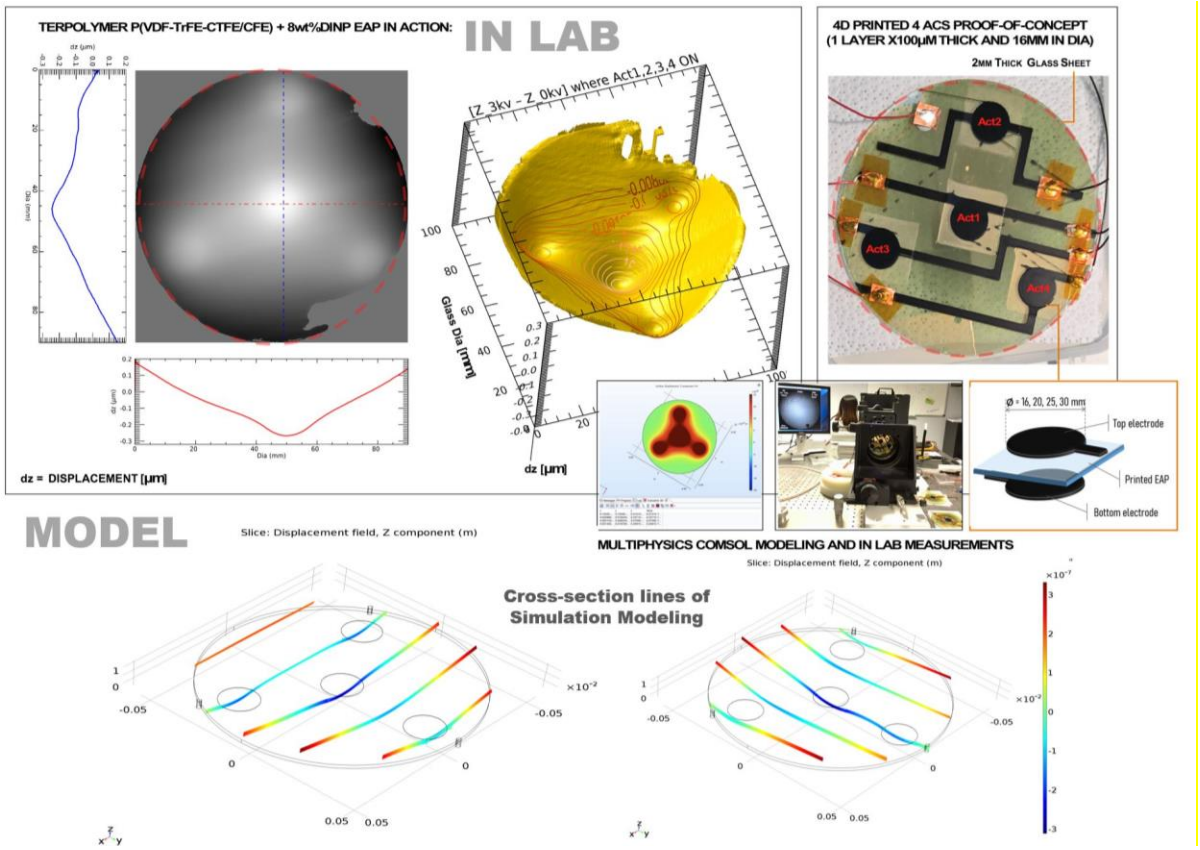

Figure 9. *The experimental control surface: Sc (front glass) measurement of the full-printed 4-multi actuator prototype. The evaluation of surface deformation was obtained from interference fringes providing the surface plot (black and white deformation graph and 3D-surface yellow graph) accompanied by COMSOL simulation modeling that is coherent in empirical results. The float glass substrates are 110 mm in diameter and 2 mm thick. Fringe measurements are accomplished by a Fizeau-type laser interferometer (Zygo Verifire™).*

In Figure 9, surface displacement (**dz**) is between 0.05 to 2.00 μm during the application of an electric field (E = 30 V/ μm). The electrode size (diameter and thickness) and construction configuration (single layer and/or multilayer) were also measured. Figure 10 and 11 show the S_c deformation when the sample was subjected to the DC voltage input. Naturally, a larger electrode and a multilayers force actuator can produce larger surface deformation **dz**. However, the multilayer structure was fabricated using the shear-mode and can be limited by its number of actuator layers, which is generated by the non-transferable shear force from the top layer and/or actuator interlayer clamping. This influence would make the glass deformation reach a *saturation regime*. Despite that, a stronger electric field can drive the EAP actuator to create higher transversal strain as well as reinforce the ability to transfer shear force from the top EAP layer in the multilayer structure.

The shear actuator seems to deform the glass locally in consonance with its shape. Thetpraphi *et al.* [11] has reported that dielectric permittivity as a function of an applied electric field can be modeled via Debye/Langevin formalism, which enabled the possibility to predict the actuation ability of electrostrictive effects in modified terpolymer composite. The success of the modeling leans on COMSOL Multiphysics® software used Debye/Langevin formalism and provided impressive glass deformation modeling results resembling the experimental measurement analysis (Figure 12). The spatial optimized simulation corroborates the related deformation magnitude and also demonstrated harmonized cross-section curvatures considering the four activated actuator prototypes (Figure 9). The appeal of these simulated and experimental models (Figure 9 to 12) goes beyond scientific difficulties and carefully unravels the electromechanical behavior of the terpolymer/plasticizer composite.

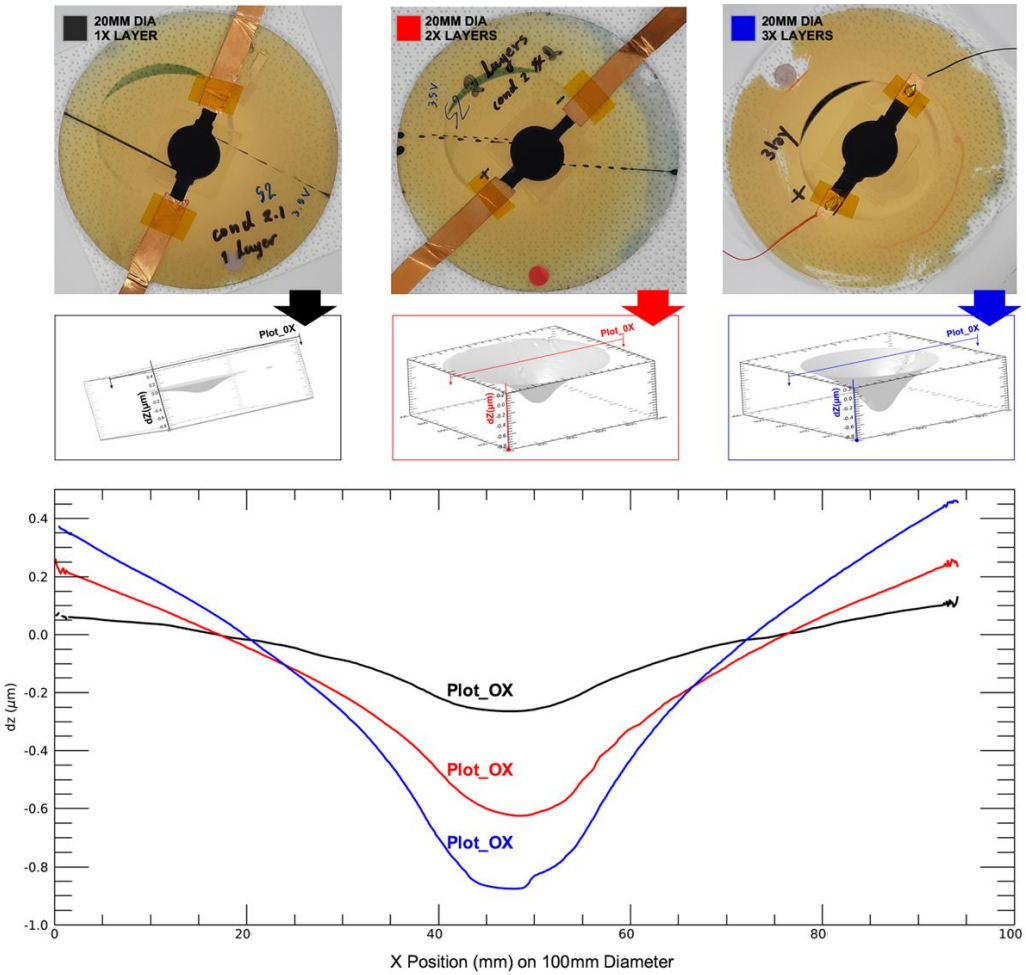

Figure 10. *The control surface (S_c) deformation represents the actuated regime under a 30 V/μm applied electric field of multilayer sample (1 actuator of 20 mm diameter) that consists of 1 layer (black), 2 layers (red), and 3 layers (blue), respectively.*

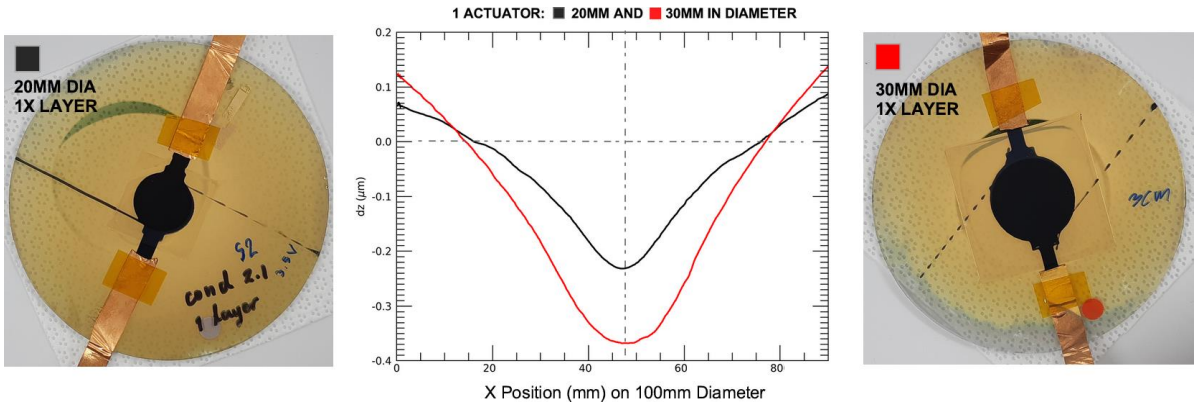

Figure 11. *The control surface (S_c) deformation represents the actuated regime (X-cross section) under a 30 V/μm applied electric field of a single-layer actuator prototype (1 actuator, 1 layer) with a 20 mm diameter (black) and a 30 mm diameter (red), respectively.*

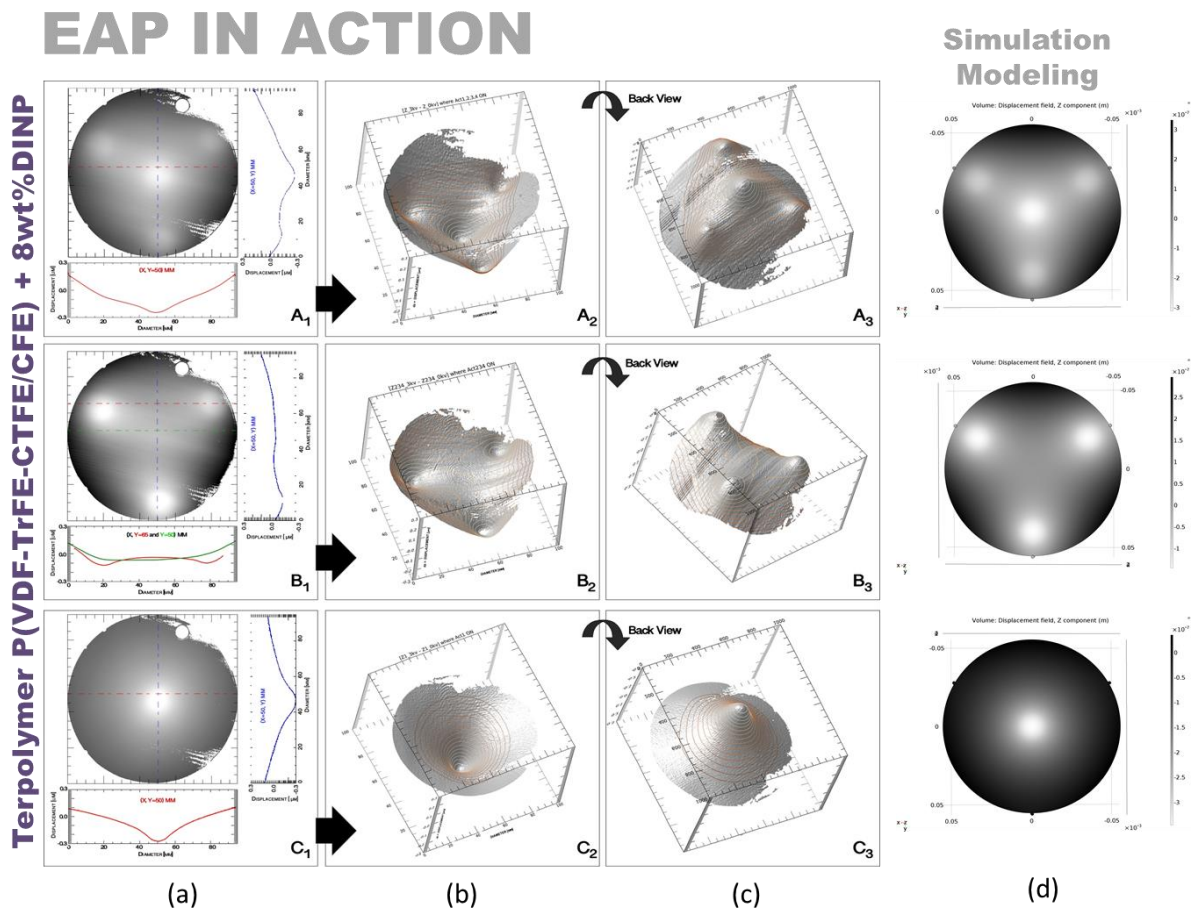

Figure 12. *The control surface (S_c) deformation with their cross-section [(X, Y), dZ] of the single-layer multi-actuator prototype with 16-mm-diameter electrodes driven by a 30 V/μm electric field. Black and white illustrations show the control surface buckling comparing between experimental results and simulation models: row (a) illustrated the deformation scale plotted with their cross-section [X,dZ] and [Y,dZ] lines, respectively; row (b) and (c) displayed the 3D surface plot of front and backside of the control surface, respectively; and row (d) describes COMSOL simulations of glass surface deformation under similar conditions.*

Table 1 shows the maximum deformation of the front glass surface generated by shear EAP to optimize the EAP sizes as well as the number of layers of the multilayer structure. Each measurement averages from 5 samples, together with the standard deviation provided in Table 1, confirming very small dispersion of the measured data. As expected, the higher displacement induces to smaller variation coefficient, i.e., defined as the SD over the mean value. This, to some extent, is reflected by the less dispersion of measures performed on the 5 tested samples when being subjected to a higher applied electric field. On the other hand, with a very low input electric field (e.g., 10V/μm), as the samples deform very little, measurement in displacement with high precision becomes challenging. For instance, it has been pointed out in practice that for a sample of 20 mm diameter, a small displacement of 0.061 μm leads to a significant error of around 24%, while only 7.2% in the case of 0.705 μm. Both experimental and modeling displacement of all prototypes depend on actuator size and number of multilayers and coincide with a range of inaccuracy measurements. Note that the surface maximum deformation in Figure 13(a) increases proportionally to an external applied electric field (E) as well as EAP actuator size (diameter & thickness). Figure 13(b) & (c) compare actuation displacements from two methods of predicting model values (COMSOL™) and measurements (maximum S_c deformation).

Table 1 indicated that the evaluation model results are very close to the empirical data (around 94-99%) in the case of varying electrode sizes. This small discrepancy is possibly originated from Ohmic heating because the composite electrode layer has low conductivity (high resistivity) versus an ideal conductive electrode (e.g., gold electrode). This resistive heat can indeed impact glass deformation especially in the particular case of large electrode areas having a higher amount of leakage current (Figure 13(b)).

The multilayer actuator has a controversy of observed displacement against the empirical model in Figure 13(c). Thetpraphi *et al.* [11] reported that EAP pre-polish shear actuators can facilitate strain-generated transfer onto the glass at certain sample thicknesses. The main attribution parameters disrupting an actuation efficiency in the real-scale experiment might come from the rough interface and the stresses in the layers [35] especially the 3D printed multilayer topology. This inter-stress in multiple-layered structures impedes the effort to reinforce transferable transversal strain by increasing the number of layers. The interlayer stress algorithm of the multilayer structure must be re-optimized in future modeling to have a better accurate model prediction performance.

Table 1. *The maximum displacement at the central S_c as measured by interferometric dynamic calibrator (in lab measurements) and COMSOL™ model evaluation (modelization & simulation) as a function of applied electric fields, actuator size, and the number of layers.*

E (V/µm)	Maximum Displacement (µm)																	
	1 layer												2 layers			3 layers		
	ø 16 mm			ø 20 mm			ø 25 mm			ø 30 mm			ø 20 mm					
	Exp.	± µm	Model	Exp.	± µm	Model	Exp.	± µm	Model	Exp.	± µm	Model	Exp.	± µm	Model	Exp.	± µm	Model
10	0.050	0.018	0.058	0.061	0.015	0.083	0.180	0.030	0.118	0.230	0.055	0.155	0.230	0.012	0.173	0.278	0.014	0.267
15	0.125	0.021		0.173	0.031		0.300	0.034		0.440	0.055		0.390	0.020		0.525	0.026	
20	0.185	0.024	0.194	0.284	0.039	0.278	0.435	0.038	0.392	0.630	0.045	0.515	0.555	0.028	0.575	0.777	0.039	0.888
25	0.244	0.027		0.350	0.055		0.565	0.042		0.830	0.080		0.745	0.037		1.010	0.051	
30	0.305	0.03	0.343	0.476	0.044	0.490	0.710	0.046	0.693	0.980	0.055	0.910	0.975	0.049	1.015	1.350	0.068	1.568
35	0.375	0.034		0.530	0.06		0.850	0.051		1.175	0.055		1.193	0.060		1.564	0.078	
40	0.445	0.037	0.475	0.705	0.051	0.678	1.025	0.056	0.959	1.400	0.080	1.260	1.493	0.075	1.405	1.838	0.092	2.170

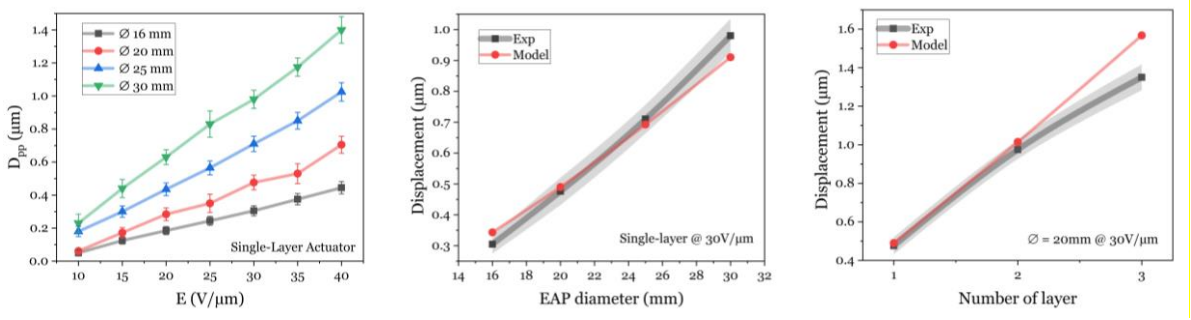

(A) **(B)** **(C)**

Figure 13. (A) *Experimental maximum displacement as a function of electric fields of the full-printed single-layer sample with different diameter sizes. Comparison between experimental measure and modeling analysis of the same sample under a 30 V/µm electric field in terms of displacement versus* ***(B)*** *EAP diameter sizes and* ***(C)*** *the number of layers.*

These results allow the assessment of this extensive actuator assembly. However, one must remember the homogeneous solvent evaporative control and stress distribution on the surface and between the interlayer and buckle delamination. Such fabrication process control is critical for an optimized mechanism. Figure 9 and Figure 12 show experimental results and confirm the compliance between electrode shape and glass optical surface deformations under an applied electric field (E=30 V/µm). Such a conclusive result paves the way for the next generation of 3D-printed multi EAP force-actuators, which

are a crucial part of hybrid dynamic structures for quality optical surface shape control, i.e, *electrical polishing* for Live-Mirror.

To assess the reliable operation of the live mirror under an applied high voltage, an actuation test consisting of 120 cycles was performed on a full-printed single-layer sample with a 20mm-diameter. Note that this tested sample was fabricated last year and was left at room temperature for 12 months. Figure 14 (A) displays the time evolution of the central displacement of S_c when being subjected to an alternating electric field of 15 V/µm amplitude and 0.1 Hz frequency. As observed, the sample provided a satisfactory actuation response for 20 minutes and seems to be unchanged in terms of electromechanical properties even 1 year after the fabrication. The small variation of the displacement (peak-to-peak) amplitude is demonstrated in Figure 14 (B). This result confirms the reliability of using the full-printed EAP actuator for several actuation cycles as well as the long-time storage possible. Last but not least, the implications of the physical aging of our advanced EAP actuator will be considered when assessing its long-term stability under several conditions, e.g., temperature, humidity, high-frequency operation, etc.

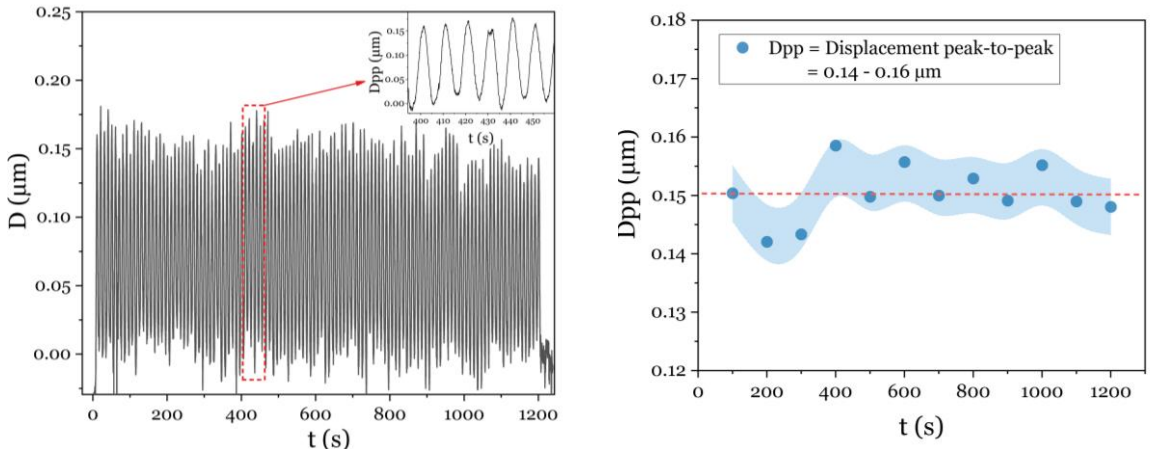

Figure 14. *The test of 120 actuation cycles (sinusoidal electric field of 15 V/µm, 100 mHz) on a 20mm-diameter full-printed single-layer sample: (A) the real-time displacement measurement, and (B) the displacement peak-to-peak value with an area error considered as the central displacement of Sc.*

IV. Conclusion

The Live-Mirror was prototyped from lab-scale fabrication for a breakthrough in automated production via additive manufacturing. The extrusion/3D printing technique underscores the feasibility of scale-up in a conventional EAP fabrication process. This offers a more automatic soft actuator fabrication suited for active optical applications. The printable advanced EAP and its compatible electrode (the optimized terpolymer carbon black composite) led to a full-printed actuator qualifying as a Live-Mirror 3D printed prototype. Modeling with COMSOL Multiphysics® showed an admirable result in excellent agreement with the experimental measurements. 3D printed actuator technology could offer several opportunities to create unique soft actuator applications like system controlling receiver mirrors for astronomy and communication systems as well as many other modern electronic devices.

To enhance the electrical conductivity of the printable electrode, a new process relying on dielectrophoresis of terpolymer/CB composite will be investigated, allowing to create alignment of anisotropic particles. This architecture favors the electrical conduction pathway, making it possible to avoid resistive self-heating under high voltage operation. Another alternative consists of using other conductive

particles with high shape anisotropy, such as fiber or flake shape. As a next step, the results motivate the development of a hybrid electrode pattern, in which an electrical connecting path (e.g., Ag ink) linked with the conductive polymer composite (CB), successfully used for a large optical area.

Future work will include the mirror surface combined with the particular shape of the EAP actuator designed to achieve local surface correction. Simultaneously, the curvature of a glass sample without EAP curvature distortion will be studied in detail to estimate the electrode and approximate the local glass curvature with an EAP electrode geometry. Both experiments and models will be determined. Moreover, we aim to scale up the Live-Mirror prototype for challenging real-scale receiver mirror production.

Acknowledgments

This project is sponsored by ANR (The French National Research Agency): Project #ANR-18-CE42-0007-01 (Live-Mirror project). Thetpraphi acknowledges the support from the DPST Thai scholarship jointly administered by the Ministry of Education and the Institute for the Promotion of Teaching Science and Technology Thailand, and the Franco-Thai Scholarship (2016) from Campus France. The authors thank INSA-Lyon for supporting the grant to invite Prof. Jeff Kuhn and Institute Carnot for their financial support. The authors also thank Asst. Prof. Chatchai Putson for assistance with Thai internships (S. Chaipo and W. Kanlayakan).

References

[1] D. Grinberg, S. Siddique, M.Q. Le, R. Liang, J.F. Capsal, P.J. Cottinet, 4D Printing based piezoelectric composite for medical applications, J. Polym. Sci. Part B Polym. Phys. 57 (2019) 109–115. https://doi.org/10.1002/polb.24763.

[2] Z. Xiang, V. Nguyen, B. Ducharne, N. Della Schiava, J. Capsal, P. Cottinet, M. Le, 3D Printing of Flexible Composites via Magnetophoresis: Toward Medical Application Based on Low-Frequency Induction Heating Effect, Macromol. Mater. Eng. 2100211 (2021) 2100211. https://doi.org/10.1002/mame.202100211.

[3] S.Z. Guo, K. Qiu, F. Meng, S.H. Park, M.C. McAlpine, 3D Printed Stretchable Tactile sensors, Adv. Mater. 29 (2017) 1–8. https://doi.org/10.1002/adma.201701218.

[4] O.F. Emon, F. Alkadi, D.G. Philip, D. Kim, K. Lee, Multi-material 3D printing of a soft pressure sensor, Addit. Manuf. 28 (2019) 629–638. https://doi.org/10.1016/j.addma.2019.06.001.

[5] V.C.F. Li, C.K. Dunn, Z. Zhang, Y. Deng, H.J. Qi, Direct Ink Write (DIW) 3D Printed Cellulose Nanocrystal Aerogel Structures, Sci. Rep. 7 (2017) 1–8. https://doi.org/10.1038/s41598-017-07771-y.

[6] S.H. Park, R. Su, J. Jeong, S.Z. Guo, K. Qiu, D. Joung, F. Meng, M.C. McAlpine, 3D Printed Polymer photodetectors, Adv. Mater. 30 (2018) 1–8. https://doi.org/10.1002/adma.201803980.

[7] G. Haghiashtiani, E. Habtour, S.H. Park, F. Gardea, M.C. McAlpine, 3D printed electrically-driven soft actuators, Extrem. Mech. Lett. 21 (2018) 1–8. https://doi.org/10.1016/j.eml.2018.02.002.

[8] B. Sparrman, C. Pasquier, S. Darbari, R. Rustom, K. Shea, S. Tibbits, Printed silicone pneumatic actuators for soft robotics, Addit. Manuf. (2021) 101860. https://doi.org/10.1016/j.addma.2021.101860.

[9] Additive manufacturing, GE Addit. (2019). https://www.ge.com/additive/additive-manufacturing (accessed May 8, 2019).

[10] K. Thetpraphi, M.Q. Le, A. Houachtia, P. Cottinet, L. Petit, D. Audigier, J. Kuhn, G. Moretto, J. Capsal, Surface Correction Control Based on Plasticized Multilayer P(VDF-TrFE-CFE) actuator—Live Mirror, Adv. Opt. Mater. 1900210 (2019) 1900210. https://doi.org/10.1002/adom.201900210.

[11] K. Thetpraphi, S. Chaipo, W. Kanlayakan, P.-J. Cottinet, M.Q. Le, L. Petit, D. Audigier, J. Kuhn, G. Moretto, J.-F. Capsal, Advanced Plasticized Electroactive Polymers Actuators for Active Optical Applications: Live Mirror, Adv. Eng. Mater. 22 (2020) 1901540.

[12] Hyrel 3D, Hyrel 3D SYSTEM 30M, (2019). http://www.hyrel3d.com/portfolio/system-30m/ (accessed February 24, 2020).

[13] S.C. Ligon, R. Liska, J. Stampfl, M. Gurr, R. Mülhaupt, Polymers for 3D Printing and Customized Additive Manufacturing, Chem. Rev. 117 (2017) 10212–10290. https://doi.org/10.1021/acs.chemrev.7b00074.

[14] A.L. Dearden, P.J. Smith, D. Shin, N. Reis, B. Derby, P.O. Brien, A low curing temperature silver ink for use in ink-jet printing and subsequent production of conductive tracks, Macromol. Rapid Commun. 26 (2005) 315–318. https://doi.org/10.1002/marc.200400445.

[15] L. V Kayser, M.D. Russell, D. Rodriquez, S.N. Abuhamdieh, C. Dhong, S. Khan, A.N. Stein, J. Ram, D.J. Lipomi, RAFT Polymerization of an Intrinsically Stretchable Water-Soluble Block Copolymer Sca ff old for PEDOT, Chem. Mater. 30 (2018) 4459–4468.

https://doi.org/10.1021/acs.chemmater.8b02040.

[16] C. Cochrane, V. Koncar, M. Lewandowski, C. Dufour, Design and Development of a Flexible Strain Sensor for Textile Structures Based on a Conductive Polymer Composite, Sensors. 7 (2007) 473–492.

[17] N. Kumar, P.K. Jain, P. Tandon, P.M. Pandey, Additive manufacturing of flexible electrically conductive polymer composites via CNC-assisted fused layer modeling process, J. Brazilian Soc. Mech. Sci. Eng. 40 (2018) 175. https://doi.org/10.1007/s40430-018-1116-6.

[18] A. Materials, Float Glass - Properties and Applications, (n.d.). https://www.azom.com/properties.aspx?ArticleID=89 (accessed May 6, 2021).

[19] K. Thetpraphi, G. Moretto, J.R. Kuhn, P.-J. Cottinet, M.Q. Le, D. Audigier, L. Petit, J. Capsal, Live-mirror shape correction technology operated through modified electroactive polymer actuators, Proc. SPIE. (2019). https://doi.org/10.1117/12.2514229.

[20] G. Cummins, M.P. Desmulliez, Inkjet printing of conductive materials : a review, Circuit World. (2012). https://doi.org/10.1108/03056121211280413.

[21] N. Della Schiava, K. Thetpraphi, M.Q. Le, P. Lermusiaux, A. Millon, J.-F. Capsal, P.-J. Cottinet, Enhanced figures of merit for a high-performing actuator in electrostrictive materials, Polymers (Basel). 10 (2018) 1–15. https://doi.org/10.3390/polym10030263.

[22] J.-F. Capsal, J. Galineau, M. Lallart, P.-J. Cottinet, D. Guyomar, Plasticized relaxor ferroelectric terpolymer: Toward giant electrostriction, high mechanical energy and low electric field actuators, Sensors Actuators, A Phys. 207 (2014) 25–31. https://doi.org/10.1016/j.sna.2013.12.008.

[23] X. Yin, J.-F. Capsal, D. Guyomar, A comprehensive investigation of poly(vinylidene fluoride- trifluoroethylene-chlorofluoroethylene) terpolymer nanocomposites with carbon black for electrostrictive applications, Appl. Phys. Lett. 104 (2014) 2012–2017. https://doi.org/10.1063/1.4864160.

[24] N. Della Schiava, M.Q. Le, J. Galineau, F. Domingues Dos Santos, P.-J. Cottinet, J.-F. Capsal, Influence of Plasticizers on the Electromechanical Behavior of a P(VDF-TrFE-CTFE) Terpolymer: Toward a High Performance of Electrostrictive Blends, J. Polym. Sci. Part B Polym. Phys. 55 (2017) 355–369. https://doi.org/10.1002/polb.24280.

[25] X. Yin, Modification of Electrostrictive Polymers and Their Electromechanical Applications, INSA de Lyon, 2015.

[26] M. Rahaman, A. Aldalbahi, P. Govindasami, N. Khanam, S. Bhandari, P. Feng, T. Altalhi, A New Insight in Determining the Percolation Threshold of Electrical Conductivity for Extrinsically Conducting Polymer Composites through Different sigmoidal models, Polymers (Basel). 10 (2017) 527. https://doi.org/10.3390/polym9100527.

[27] Q. Zhang, J. Wang, B. Zhang, B. Guo, J. Yu, Z. Guo, Improved electrical conductivity of polymer/carbon black composites by simultaneous dispersion and interaction-induced network assembly, Compos. Sci. Technol. 179 (2019) 106–114. https://doi.org/10.1016/j.compscitech.2019.05.008.

[28] K. Thetpraphi, Development of electroactive polymer actuators for next generation mirror : Live-Mirror, Université de Lyon, 2020.

[29] F. Kremer, S. Andreas, Broadband Dielectric Measurement Techniques, Springer Science & Business Media, 2002.

[30] A. Kahouli, Spectroscopie diélectrique appliquée aux polymères, Tech. l'ingénieur Matériaux Isolants En Électrotechnique. TIB255DUO (2016). https://www.techniques-ingenieur.fr/base-documentaire/energies-th4/materiaux-isolants-en-electrotechnique-42255210/spectroscopie-dielectrique-appliquee-aux-polymeres-d2308/.

[31] J.-F. Capsal, J. Galineau, M.Q. Le, F. Domingues Dos Santos, P.-J. Cottinet, Enhanced electrostriction based on plasticized relaxor ferroelectric P(VDF-TrFE-CFE/CTFE) blends, J. Polym. Sci. Part B Polym. Phys. 53 (2015) 1368–1379. https://doi.org/10.1002/polb.23776.

[32] F. Pedroli, A. Marrani, M.Q. Le, O. Sanseau, P.-J. Cottinet, J.-F. Capsal, Reducing leakage current and dielectric losses of electroactive polymers through electro-annealing for high-voltage actuation, RSC Adv. 9 (2019) 12823–12835. https://doi.org/10.1039/c9ra01469a.

[33] M. Ben-David, L. Engel, Y. Shacham-Diamand, Spectroscopic ellipsometry study of spin coated P(VDF-TrFE-CTFE) thin films and P(VDF-TrFE-CTFE)/PMMA blends, Microelectron. Eng. 171 (2017) 37–43. https://doi.org/10.1016/j.mee.2017.01.030.

[34] D. Jeong, Electro-Optical Properties in Relaxor Ferroelectric Materials and the Device Applications, (2004) 125.

[35] S. Faulhaber, C. Mercer, M.-W. Moon, J. Hutchinson, A. Evans, Buckling delamination in compressed multilayers on curved substrates with accompanying ridge cracks, J. Mech. Phys. Solids. 54 (2006) 1004–1028. https://doi.org/10.1016/j.jmps.2005.11.005.